

Communication

# Novel Tetrazolium-Based Colorimetric Assay for Helicase nsp13 in SARS-CoV-2<sup>†</sup>

Triet M. Pham, Morgan G. Howard, Shane M. Carey , Lindsey R. Baker and Edward L. D'Antonio \* 

Department of Natural Sciences, University of South Carolina Beaufort, 1 University Boulevard, Bluffton, SC 29909, USA

\* Correspondence: edantonio@uscb.edu; Tel.: +1-843-208-8101

<sup>†</sup> Supported by the University of South Carolina, Office of the Vice President for Research, Experiment.com, and by the Shirley E. Caputo Memorial Fund within the Community Foundation of the Lowcountry to E.L.D.

**Abstract:** Severe Acute Respiratory Syndrome Coronavirus 2 (SARS-CoV-2) is a human pathogenic virus that encodes for a helicase (SC2Hel) that is essential for viral replication. SC2Hel has the ability to unravel dsRNA or dsDNA in an NTP-dependent manner from the 5' to 3' directionality. The standard helicase assay from studies involving SARS-CoV and SARS-CoV-2 have relied on the concept of fluorescence resonance energy transfer. Adding to the collection of helicase assays, herein, we have developed a novel tetrazolium-based colorimetric assay system for the detection of ADP that is produced via SC2Hel activity. This SC2Hel assay combines three enzyme-coupled steps involving the ADP-dependent *Thermococcus litoralis* glucokinase (TlGlcK), *Leuconostoc mesenteroides* glucose-6-phosphate dehydrogenase (LmG6PDH), and *Clostridium kluyveri* diaphorase (CkDIA). Iodonitrotetrazolium chloride (INT), a colorimetric tetrazolium reagent, was used in the final step of the assay that converted into INT-formazan during reduction. INT-formazan in the assay's buffered solution at pH 7.6 exhibited an intense colorimetric response at a wavelength maximum of 505 nm. The assay exhibited excellent performance characteristics as it revealed a Z' factor of 0.87 and it has the potential to be further adopted into high-throughput screening studies for therapeutic drug discovery research.



**Citation:** Pham, T.M.; Howard, M.G.; Carey, S.M.; Baker, L.R.; D'Antonio, E.L. Novel Tetrazolium-Based Colorimetric Assay for Helicase nsp13 in SARS-CoV-2. *BioChem* **2024**, *4*, 115–125. <https://doi.org/10.3390/biochem4020006>

Academic Editor: Allan Chris Ferreon

Received: 6 April 2024  
Revised: 8 May 2024  
Accepted: 13 May 2024  
Published: 15 May 2024



**Copyright:** © 2024 by the authors. Licensee MDPI, Basel, Switzerland. This article is an open access article distributed under the terms and conditions of the Creative Commons Attribution (CC BY) license (<https://creativecommons.org/licenses/by/4.0/>).

**Keywords:** SARS-CoV-2; COVID-19; nsp13; helicase; absorbance-based assay; INT

## 1. Introduction

The clinical management of Severe Acute Respiratory Syndrome Coronavirus 2 (SARS-CoV-2) infections using pharmaceutical therapeutics is an important course of action despite the large number of lives saved using vaccinations at the global scale. There is still a large number of people at risk, who will develop symptoms and may possibly die from Coronavirus Disease 2019 (COVID-19) [1,2]. With the pandemic at a close, COVID-19 will continue to ensue from the emerging variants of SARS-CoV-2. The outbreak originated in Wuhan, China in December of 2019 and the original strain of the virus (pre-global vaccination availability) was easily transmissible via human-to-human interaction. Viral transmission generally occurs via infected individuals speaking, sneezing, or coughing, in which respiratory droplets containing the virus transfer through the air while another person inhales the aerosol. Respiratory tract infections generally affect the nose, throat, sinuses, lungs, and trachea. Symptoms of COVID-19 include fever, dry cough, and fatigue. Although most people who are infected have mild symptoms and will recover, there are high-risk groups. Two of these groups include patients who are over the age of 60 years old and patients that have pre-existing medical conditions (i.e., heart failure, suppressed immune systems due to taking immunosuppressants, etc.) [2]. With only a limited number of therapeutics available for clinical use [3], such as Nirmatrelvir–Ritonavir (Paxlovid™) [4], Remdesivir [5], and Molnupiravir [6], a key starting point for early stage therapeutic drug

discovery is to focus on finding inhibitors of critically important enzymes of the virus. This can be accomplished using the molecular target-based high-throughput screening (HTS) approach to reveal potent, anti-SARS-CoV-2, hit-to-lead candidates that are not cytotoxic to host cells.

SARS-CoV-2 is a betacoronavirus that is a positive-sense ssRNA virus. It is also pathogenic to humans and it contains essential proteins involved in cell surface attachment, RNA and viral genomic replication, and translation of viral structural proteins. Once expressed in a host cell, 16 non-structural proteins (nsps) are produced [7] and these nsps represent a drug discovery targeting opportunity. One target that has received attention in previous early stage therapeutic drug discovery studies is Coronavirus non-structural protein 13 (nsp13), which is known as SARS-CoV-2 helicase (SC2Hel) [8–10]. It is highly conserved with respect to SARS-CoV helicase because between the two helicases there is a 99.8% protein sequence identity observed (100% sequence similarity) where one amino acid differs out of 601 amino acids [7]. SC2Hel serves the function of unravelling dsRNA or dsDNA in an NTP-dependent method from the 5' to 3' directionality [8,10–13]. The standard nucleic acid unwinding assay involving helicase from studies of SARS-CoV and SARS-CoV-2 encompasses the concept of fluorescence resonance energy transfer (FRET) [8,12,14,15]. Typically, in this type of assay, the FRET-based, fluorescence-quenching approach generally displays nucleic acid strand separation that is catalyzed by the helicase. The substrate structure specificity requires a 'forked' model or 5'-end, single-stranded overhang that is at least 10 bases in length [11]. Adedeji and co-workers revealed eight different duplex nucleic acid substrates for SARS-CoV helicase in a previous study [12]. This nucleic acid substrate generally has one strand containing a Cy3 fluorophore positioned at the 5' end. On the opposing strand (the quencher strand), at the 3' end there is a Black Hole Quencher-2 included for DNA or an Iowa Black RQ included for RNA. A DNA competitor strand (complementary to the Cy3 strand) is used in the assay to prevent the reannealing process of the substrate [8]. SC2Hel also involves NTPase activity and can be effectively run via ATP, but the other NTPs can also afford activity [8,11,12]. SC2Hel has an ATP-coupling stoichiometry of one ATP needed for each bp unwound [16]. NTPase activity assays have been performed using several methods. One method involves monitoring the reaction products of helicase, in which they are separated using thin-layer chromatography and observed via autoradiography through visual inspection. A quantitative analysis of inorganic phosphate released in the reaction from the hydrolysis of  $\gamma$   $^{32}$ P-ATP is performed and plotted against the reaction time [11]. Another NTPase assay involves the complexation of the released inorganic phosphate (from the NTP with helicase) with malachite green and molybdate (AM/MG reagent), which is a colorimetric method [13].

The helicase assay presented herein is based on colorimetry and probes on both nucleic acid unwinding and ATPase activities in one format. The general assay (Figure 1) involves a set of three supporting enzymes, which are coupled to the helicase reaction; therefore, a total of four enzymatic steps are required. SC2Hel has a preferred substrate consisting of a 5' single-stranded overhang 31/18-mer duplex nucleic acid (dsDNA or dsRNA) (Figure 2). The final reaction step produces a water-soluble tetrazolium chromophore, INT-formazan, that has a wavelength maximum of 505 nm in a buffered solution of pH 7.6. The assay was partly modeled from a system conceived by McFarlane and Murray [17]. Moreover, the Michaelis–Menten parameters observed from this SC2Hel–INT assay are in close agreement with values recently reported by Zeng and colleagues for a SC2Hel–FRET assay [8].

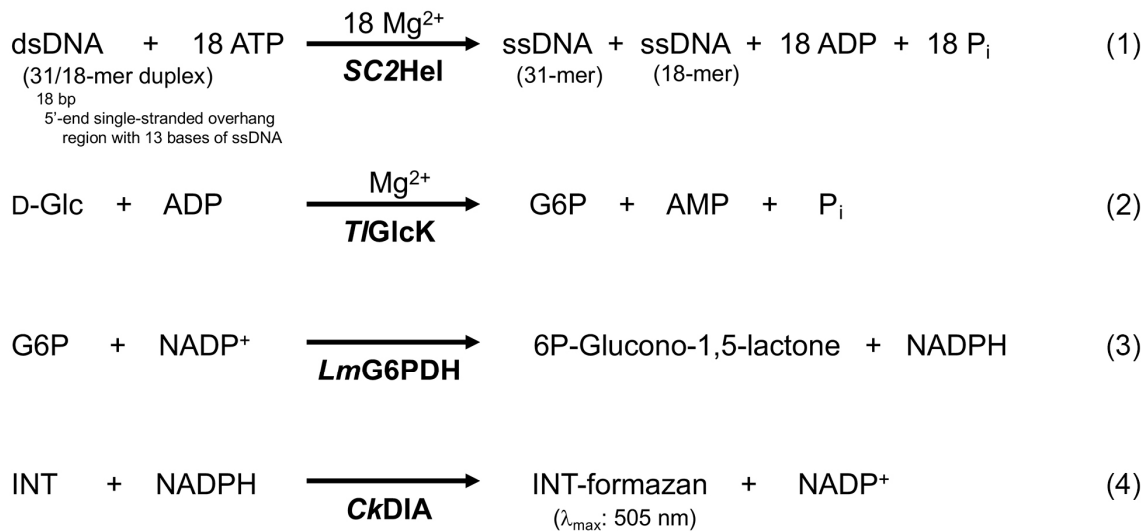


**Figure 1.** SARS-CoV-2 helicase enzyme-coupled, colorimetric-based assay utilizing INT as the colorimetric reagent, CkDIA as the electron transfer enzyme coupling reagent, and a dsDNA substrate presented as a 5' single-stranded overhang 31/18-mer (as shown in Figure 2b). Unwinding of the 31/18-mer dsDNA substrate via SARS-CoV-2 nsp13 helicase (SC2Hel) requires the energy of ATP and promotes the formation of ADP. ADP formation is followed by coupling to INT-formazan formation through the ADP-dependent *Thermococcus litoralis* glucokinase (TlGlcK), *Leuconostoc mesenteroides* glucose-6-phosphate dehydrogenase (LmG6PDH), and *Clostridium kluyveri* diaphorase (CkDIA).

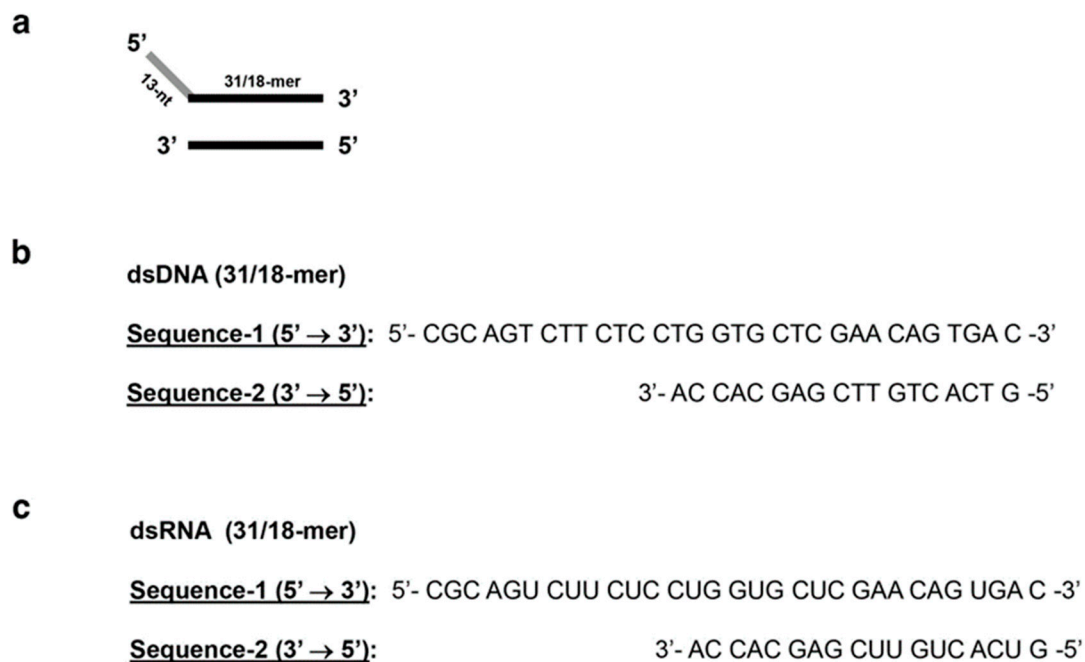


**Figure 2.** (a) Structure of a 5' single-stranded overhang 31/18-mer duplex nucleic acid substrate of SC2Hel. The 31/18-mer substrate in the forms of either (b) dsDNA or (c) dsRNA.

## 2. Materials and Methods

### 2.1. Chemicals and Reagents

The 31/18-mer duplex dsDNA was purchased from Integrated DNA Technologies. Isopropyl β-D-thiogalactopyranoside was purchased from Carbosynth. Ethylenediaminetetraacetic acid tetrasodium salt hydrate, imidazole, bovine pancreas deoxyribonuclease I (DNase I), bovine pancreas ribonuclease A (RNase A), triethanolamine, β-nicotinamide adenine dinucleotide phosphate hydrate (NADP<sup>+</sup>), adenosine 5'-triphosphate disodium salt

hydrate (ATP, >99%), iodonitrotetrazolium chloride, iodonitrotetrazolium violet-formazan, Terrific broth, kanamycin sulfate, and dimethyl sulfoxide (DMSO) were purchased from Sigma (St. Louis, MO, USA). *Clostridium kluyveri* diaphorase (CkDIA; E.C. 1.8.1.4) and *Leuconostoc mesenteroides* glucose 6-phosphate dehydrogenase (LmG6PDH; E.C. 1.1.1.49) were obtained from Worthington Biochemical Corporation (Lakewood, NJ, USA). Luria–Bertani (LB) broth, lysozyme (type VI), cobalt–nitrotriacetic acid resin, protease inhibitor tablets (EDTA-free), D-glucose, glycerol, magnesium chloride, sodium phosphate dibasic, potassium phosphate monobasic, DL-dithiothreitol, and all other chemicals were purchased from Fisher Scientific (Hampton, NH, USA).

## 2.2. Cloning

Gene synthesis was performed for the genes of *Severe Acute Respiratory Syndrome Coronavirus 2* helicase nsp13 (GenBank accession number YP\_009725308.1) and *Thermococcus litoralis* (DSM 5473) ADP-dependent glucokinase (GenBank accession number Q7M537.1) followed by cloning into separate kanamycin-resistant pET-28a(+) *Escherichia coli* expression vectors at restriction sites 5' NcoI and 3' HindIII at Azenta Life Sciences, Inc. (South Plainfield, NJ, USA). Each construct encoded for an N-terminal hexahistidine tag, such as the segment MGRGSHHHHHGMA that preceded the start methionine. Codons for both plasmids were optimized to be used in protein expression of *Escherichia coli*. The plasmid constructs were designated as pET-SC2Hel and pET-TIGlcK, respectively.

## 2.3. Expression and Purification of Recombinant SC2Hel

Transformation of the plasmid pET-SC2Hel was performed using the heat shock method using *E. coli* strain BL21(DE3) (New England Biolabs, Ipswich, MA, USA) and colonies were grown on LB agar plates with 50 µg/mL of kanamycin. Starter cultures containing 5 mL of LB broth, 50 µg/mL of kanamycin, and a single colony of *E. coli* from the transformation step were incubated at 37 °C and shaking at 250 rpm for 8 h using a New Brunswick Scientific C24 incubator shaker. The starter cultures were used to inoculate six 2 L culture flasks containing 500 mL of Terrific broth (Sigma) supplemented with 0.4% (*v/v*) glycerol and 50 µg/mL of kanamycin, followed by an incubation of 16 h at 37 °C and shaking at 220 rpm. The culture flasks used autoclaved cheesecloth lids to allow air flow. The 500 mL cultures were induced with isopropyl β-D-thiogalactopyranoside to a final concentration of 1 mM and were incubated for an additional 24 h at 28–32 °C with shaking at 220 rpm. The *E. coli* was centrifuged at 7000 rpm and the resultant cell pellet was recovered and stored at –80 °C, overnight. The frozen pellet was thawed from –80 °C to room temperature and resuspended in lysis buffer [50 mM 4-(2-hydroxyethyl)piperazine-1-ethanesulfonic acid (HEPES) (pH 7.0), 150 mM NaCl]. Cell lysis was performed by adding lysozyme and the cell suspension was stirred for 1 h at 4 °C before adding EDTA-free protease inhibitor tablets, after which the cell lysate was sonicated for 30 min in a water bath sonicator (FS20, Fisher Scientific) and stored at –20 °C overnight. The cell lysate was thawed to room temperature and DNase I (Sigma) and RNase A (Sigma) at final concentrations of 10 µg/mL and 16 µg/mL, respectively, were added and stirred at 4 °C for 1 h, followed by overnight freezing at –80 °C. The cell lysate was thawed to room temperature and centrifuged at 15,000 rpm (Sorvall RC5C Plus centrifuge, SS-34 rotor) for 45 min at 4 °C and the resulting supernatant was recovered and loaded onto a cobalt–nitrotriacetic acid (Co-NTA) immobilized-metal affinity chromatography column [1.5 cm (internal diameter) × 4.0 cm (bed height)] that was pre-equilibrated using mobile phase A1 [50 mM HEPES (pH 7.0), 300 mM NaCl]. Mobile phase A1 was used as an initial wash to aid in the elution of most protein impurities. An isocratic step was applied from 0% to 13% mobile phase B1; note: mobile phase B1 [50 mM HEPES (pH 7.0), 300 mM NaCl, 150 mM imidazole]. After UV absorbance ( $\lambda = 280$  nm) on the chromatogram reached baseline, a gradient elution from 13 to 100% mobile phase B1 (50 mL gradient) was implemented in order to elute most of the other impurities from the column. Fractions of SC2Hel resulting from the Co-NTA step were pooled, concentrated using an Amicon Ultra YM-30 centrifugal

concentrator (Millipore, Darmstadt, Germany), and buffer exchanged into mobile phase A1 using a PD-10 desalting column (GE Healthcare, Chicago, IL, USA). SC2Hel in mobile phase A1 was subjected to nucleic acid digestion using DNase I (purified from bovine pancreas that is free of any ribonucleases and proteases) and RNase A (purified from bovine pancreas that is free of deoxyribonucleases and proteases) (Worthington Biochemical Corporation). Specifically, DNase I (final concentration of 1.0 mg/mL) and RNase A (final concentration of 1.0 mg/mL) were added to the pooled fractions SC2Hel at 4 °C for 3 h. The digested sample was immediately loaded onto a Co-NTA column [1.5 cm (internal diameter) × 4.0 cm (bed height)] where the resin had never been used before. The resin was pre-equilibrated using mobile phase A1 (*vide supra*) and an isocratic step was applied from 0% to 100% mobile phase C1 [50 mM HEPES (pH 7.0), 1.0 M NaCl]. This MP-C1 (high salt concentration) wash step was implemented as a method to dissociate and elute off any interacting nucleic acids (DNA/RNA) using the helicase. A second isocratic step was applied in order to return to 100% MP-A1. Finally, a third isocratic step was applied to 100% MP-B1 to elute SC2Hel as nucleic acid free. Fractions of SC2Hel were pooled and concentrated to 5 mL using an Amicon Ultra YM-30 centrifugal concentrator (Millipore). The sample was loaded onto a 16/600 size-exclusion column (GE Healthcare) that had been pre-equilibrated using filtered mobile phase A2 [50 mM triethanolamine (pH 7.6), 150 mM NaCl], which was the required buffer solution for the assay experiments (*vide infra*). Sodium dodecyl sulfate–polyacrylamide gel electrophoresis revealed the final fractions to be approximately 98% pure, via visual inspection. The pure fractions were pooled and concentrated to 0.16 mg/mL ( $2.34 \times 10^{-6}$  mol/L) [ $\epsilon_{280} = 68,785 \text{ M}^{-1} \text{ cm}^{-1}$  [18]; M.W. = 68,425 g/mol (monomer of His-tagged SC2Hel)]. UV–visible spectrophotometry revealed an absorbance maximum at 280 nm (as opposed to 260 nm) for SC2Hel, indicating that nucleic acid digestion was accomplished.

#### 2.4. Expression and Purification of Recombinant TIGlcK

Transformation of the plasmid pET-TIGlcK was performed using the heat shock method using *E. coli* strain BL21(DE3) (New England Biolabs) and colonies were grown on LB agar plates with 50 µg/mL of kanamycin. Starter cultures containing 5 mL of LB broth, 50 µg/mL of kanamycin, and a single colony of *E. coli* from the transformation step were incubated at 37 °C and shaken at 250 rpm for 8 h using a New Brunswick Scientific C24 incubator shaker. The starter cultures were used to inoculate six 2 L culture flasks containing 500 mL of Terrific broth modified (Sigma) supplemented with 0.4% (*v/v*) glycerol and 50 µg/mL of kanamycin, followed by an incubation of 16 h at 37 °C and shaking at 220 rpm. The culture flasks used autoclaved cheesecloth lids to allow air flow. The 500 mL cultures were induced using isopropyl β-D-thiogalactopyranoside to a final concentration of 1 mM and were incubated for an additional 24 h at 28–32 °C with shaking at 220 rpm. The *E. coli* was centrifuged at 7000 rpm where the resultant cell pellet was recovered and stored at –80 °C overnight. The frozen pellet was thawed from –80 °C to room temperature and resuspended in lysis buffer [50 mM 4-morpholinepropanesulfonic acid (pH 7.0), 150 mM NaCl]. Cell lysis was performed by adding lysozyme and the cell suspension was stirred for 1 h at 4 °C before adding EDTA-free protease inhibitor tablets, after which the cell lysate was sonicated for 30 min in a water bath sonicator (FS20, Fisher Scientific) and stored at –20 °C overnight. The cell lysate was thawed to room temperature and DNase I and RNase A (both enzymes from Sigma) at final concentrations of 10 µg/mL and 16 µg/mL, respectively, were added and stirred at 4 °C for 1 h, followed by overnight freezing at –80 °C. The cell lysate was thawed to room temperature and centrifuged at 15,000 rpm (Sorvall RC5C Plus centrifuge, SS-34 rotor) for 45 min at 4 °C and the resulting supernatant was recovered and loaded onto a Co-NTA immobilized-metal affinity chromatography column [1.5 cm (internal diameter) × 4.0 cm (bed height)] that was pre-equilibrated using mobile phase A1 [50 mM HEPES (pH 7.0), 300 mM NaCl]. Mobile phase A1 was used as an initial wash to aid in eluting protein impurities followed by an isocratic step to 13% mobile phase B1; note: mobile phase B1 [50 mM HEPES (pH 7.0), 300 mM NaCl, 150 mM

imidazole]. After UV absorbance ( $\lambda = 280$  nm) on the chromatogram reached baseline, a gradient elution from 13 to 100% mobile phase B1 (50 mL gradient) was implemented in order to elute most of the other impurities from the column. Fractions of *TlGlcK* resulting from the Co-NTA step were pooled and concentrated to 5 mL using an Amicon centrifugal concentrator (Millipore) equipped with a YM-30 membrane (30 kDa MWCO). The sample was loaded onto a 16/600 size-exclusion column (GE Healthcare) that was pre-equilibrated using filtered mobile phase A2 [50 mM triethanolamine (pH 7.6), 150 mM NaCl], which was the required buffer solution for the assay experiments (*vide infra*). A visual inspection analysis of sodium dodecyl sulfate–polyacrylamide gel electrophoresis revealed the final fractions to be >99% pure. The pure fractions were pooled and concentrated to 1.0 mg/mL [ $\epsilon_{280} = 50,310 \text{ M}^{-1} \text{ cm}^{-1}$  [18]; M.W. = 55,192 g/mol (monomer of His-tagged *TlGlcK*)].

### 2.5. Colorimetric-Based Nucleic Acid Unwinding Assay Using *SC2Hel* and *INT*

Observing enzymatic activity of *SC2Hel* in order to produce a Michaelis–Menten plot was performed using the following protocol. In brief, a four-enzyme colorimetric assay was performed (Figure 1). The assay is based on the formation of INT-formazan in aqueous buffered solution at pH 7.6 ( $\lambda_{\text{max}} = 505$  nm). In the first step of the assay, *SC2Hel* in the presence of an overhang dsDNA substrate called 31/18-mer dsDNA (Figure 2b) and ATP react to form a 31-oligomer ssDNA, an 18-oligomer ssDNA, and ADP (note: a similar dsRNA substrate could also be used, as shown in Figure 2c). In the second step, *TlGlcK* in the presence of the formed ADP and D-glucose react to form G6P and AMP. In the third step, *LmG6PDH* in the presence of the formed G6P and  $\text{NADP}^+$  react to form 6-phospho-glucono-1,5-lactone and NADPH. Finally, in the fourth step, *CkDIA* in the presence of the formed NADPH and INT (Figure 3a) react to form  $\text{NADP}^+$  and INT-formazan (Figure 3b). INT-formazan has a UV–visible spectrophotometric absorption at a wavelength maximum of 505 nm. All measurements were performed in triplicate. In a given assay reaction mixture, the total volume was 168  $\mu\text{L}$ , and the following shows typical final assay concentrations (F.A.C.s) used in the assays. F.A.C.s for enzymes: *SC2Hel* (0.89  $\mu\text{g}/\text{mL}$  (or)  $1.3 \times 10^{-8}$  mol/L), *TlGlcK* (6.0  $\mu\text{g}/\text{mL}$ ), *LmG6PDH* (6.0  $\mu\text{g}/\text{mL}$ ), and *CkDIA* (0.6 U/mL). F.A.C.s for reagents: dsDNA substrate [31/18-mer dsDNA] (Figure 2b) (range of 0.625  $\mu\text{M}$ –20.0  $\mu\text{M}$ ), assay buffer [50 mM triethanolamine (pH 7.6), 150 mM NaCl], D-glucose (1.9 mM),  $\text{NADP}^+$  (0.51 mM),  $\text{MgCl}_2$  (7.8 mM), INT (0.60 mM), DMSO (1.0% by volume), and ATP (2.0 mM). A typical reaction involved combining all enzyme solutions with all reagent solutions (*vide supra*) except that the reaction was started by adding ATP. Once initiated, the four-enzyme reaction was carried out progressively, as shown in Figure 1. Reactions had a run time of 10.0 min, a temperature of 22 °C, and were run in the dark (left within the microplate reader after initiation). Note: a fresh solution of ATP should be used and kept on ice for no longer than 60 min to prevent autohydrolysis degradation of ATP to form ADP, which would cause a false-positive signal in the assay. For quantification of INT-formazan, UV–visible spectrophotometric absorbance readings were recorded at 505 nm ( $\lambda_{\text{max}}$ ) using a Tecan Spectrofluor Plus microplate reader in absorbance mode. A stock standard solution of 3.700 mM INT-formazan in 100% DMSO was prepared followed by mixing 25  $\mu\text{L}$  into 175  $\mu\text{L}$  of DMSO and performing a serial dilution, where each dilution divided the concentration by two. Each serial diluted standard was mixed with buffer [50 mM TEA (pH 7.6), 150 mM NaCl] as a 1:1 mixture to ensure an overall pH of 7.6. A standard curve was implemented for INT-formazan (relative absorbance vs. [INT-formazan]) at pH 7.6, in which the standard solutions of INT-formazan had a concentration range from 0.0018 to 0.2313 mM.

### 2.6. Colorimetric-Based ATPase Assay Using *SC2Hel* and *INT*

The ATPase assay was performed in a similar manner to the nucleic acid unwinding assay (*vide supra*) except that the F.A.C. for the dsDNA substrate [31/18-mer dsDNA] was set to a value of 72.0  $\mu\text{M}$  and ATP was used in a concentration range of 0.0156–1.00 mM.

Reactions were initiated using SC2Hel, has a reaction time of 10.0 min, had a temperature of 22 °C, and were run in the dark (left within the microplate reader after initiation).

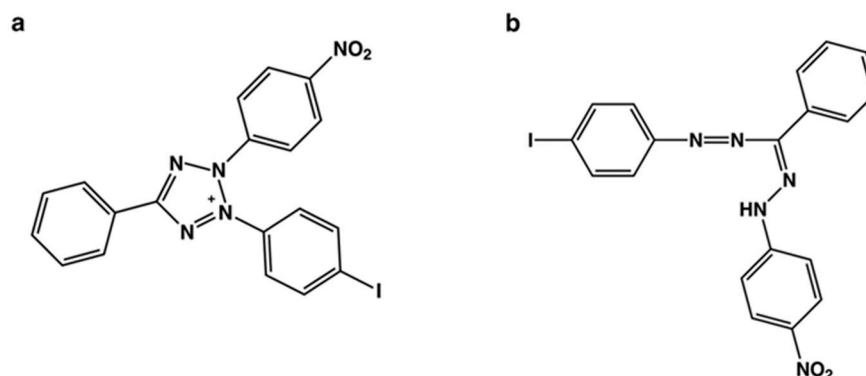


**Figure 3.** Chemical structures of the oxidized and reduced forms of INT. (a) INT (oxidized form) is a colorimetric reagent that becomes reduced by CkDIA and NADPH to form (b) INT-formazan (reduced form) with strong absorption of visible light at  $\lambda_{\max} = 505$  nm.

### 2.7. Optimization of the Incubation Time and Quantity of SC2Hel for the Assay

In order to determine a satisfactory quantity of enzyme to use in the SC2Hel assay, absorption of INT-formazan at  $\lambda_{\max} = 505$  nm was measured using an Agilent 8453 UV–visible spectrophotometer in the presence of various combinations of enzyme amounts (0.4, 2, 4, and 8  $\mu\text{g}$  per reaction) and an incubation time course ranging from 32 to 872 s at room temperature (22 °C). The assay protocol described in Section 2.5 was followed in order to carry out this determination (*vide supra*).

### 2.8. Z' Factor Determination

In order to determine the Z' factor for the SC2Hel assay, there was an incubation time of 600 s, the assay was performed at room temperature, absorbance was monitored at 505 nm using a VANTastar-F multimode microplate reader (BMG-Labtech), and all measurements were performed in septuplet. Furthermore, in a given assay reaction mixture for the positive controls, the following solution volumes and concentrations of reagents were added, as follows: (a) 55.7  $\mu\text{L}$  of buffer A [50 mM TEA (pH 7.6), 150 mM NaCl], (b) 29.3  $\mu\text{L}$  of 10 mM D-glucose, (c) 4.7  $\mu\text{L}$  of 17 mM NADP<sup>+</sup>, (d) 9.4  $\mu\text{L}$  of 124 mM MgCl<sub>2</sub>, (e) 9.4  $\mu\text{L}$  of 10 mM INT in 100% DMSO, (f) 20.0  $\mu\text{L}$  of 0.40 mg/mL SC2Hel in buffer A, (g) 0.94  $\mu\text{L}$  of 1.0 mg/mL TlGlcK in buffer A, (h) 0.94  $\mu\text{L}$  of 1.0 mg/mL LmG6PDH in buffer A, (i) 0.94  $\mu\text{L}$  of 2.72 mg/mL diaphorase in buffer A, (j) 18.8  $\mu\text{L}$  of 160.0  $\mu\text{M}$  dsDNA (31/18-mer) in buffer A, and (k) 17.6  $\mu\text{L}$  of 17 mM ATP. In the case of preparing a given reaction mixture for a negative control (also performed in septuplet), the following solution volumes and concentrations of reagents were added, as follows: (a) 94.4  $\mu\text{L}$  of buffer A, (b) 29.3  $\mu\text{L}$  of 10 mM D-glucose, (c) 4.7  $\mu\text{L}$  of 17 mM NADP<sup>+</sup>, (d) 9.4  $\mu\text{L}$  of 124 mM MgCl<sub>2</sub>, (e) 9.4  $\mu\text{L}$  of 10 mM INT in 100% DMSO, (f) 0.94  $\mu\text{L}$  of 1.0 mg/mL TlGlcK in buffer A, (g) 0.94  $\mu\text{L}$  of 1.0 mg/mL LmG6PDH in buffer A, (h) 0.94  $\mu\text{L}$  of 2.72 mg/mL diaphorase in buffer A, and (i) 17.6  $\mu\text{L}$  of 17 mM ATP. Negative controls lacked both SC2Hel and dsDNA (31/18-mer) where the total volume was adjusted by adding buffer A. Exclusion of either component alone would also produce the exact same negative control result.

## 3. Results and Discussion

### 3.1. Determination of the Optimal Incubation Time and Quantity of SC2Hel for the Assay

The study began with the monitoring of the UV–visible absorption spectra for INT-formazan production from the SC2Hel assay (at room temperature) performed by using 8  $\mu\text{g}$  of SC2Hel enzyme at various scanned time points (32, 152, 272, 392, 512, 632, 752, and 872 s) (Figure 4a). When analyzed as the  $\lambda_{\max}$  of INT-formazan (505 nm) as a function of time (Figure 4b), a tangent line is observed to run through data points ranging from 32 to

512 s with a high  $R^2$  value of 0.9995, after which the time trace slightly loses its linearity. The time point of 632 s is at a 5.9% deviation loss from the tangent line. Consequently, we selected a slightly shorter timing of 600 s to be within a 5% error and to be used for our time optimum at room temperature. Through optimization of the incubation time concerning the linear regime of the enzymatic reaction, the steady-state activity was maintained and allowed for the observation of good Michaelis–Menten curves and corresponding parameters (*vide infra*).

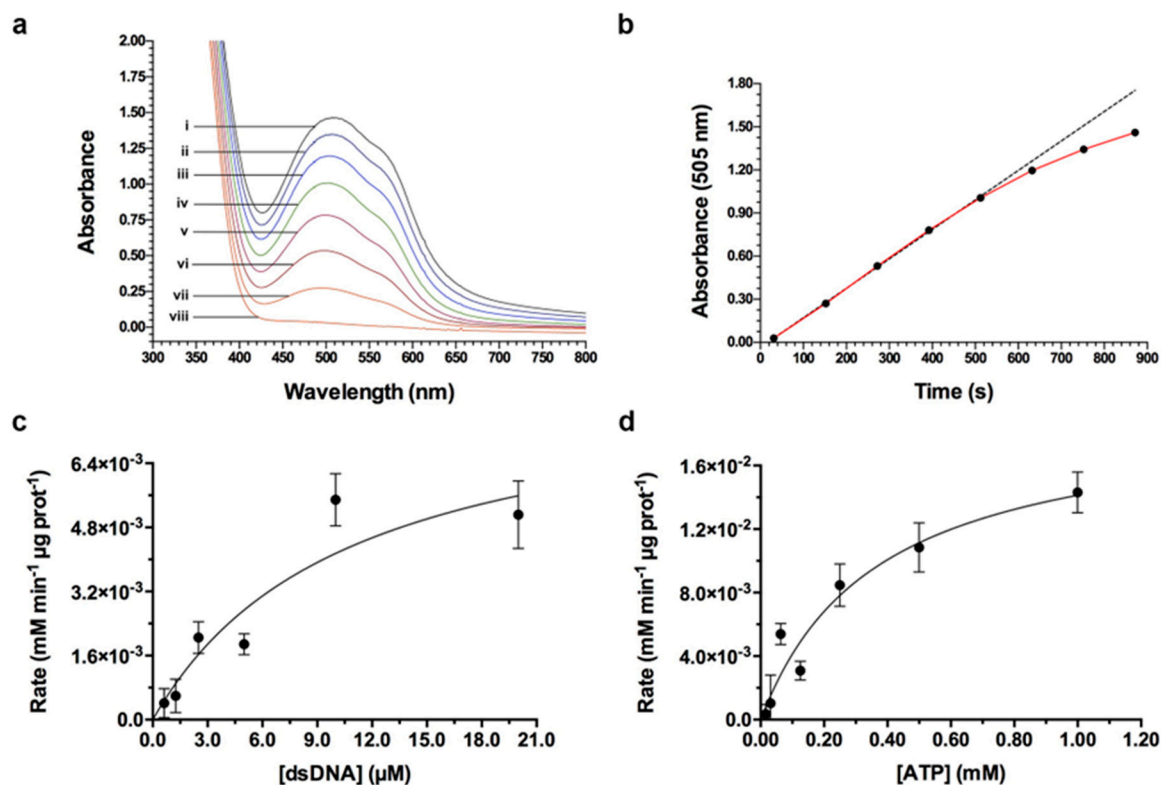


**Figure 4.** Kinetics of the SC2Hel/INT assay. The time optimum determination was assessed for the general assay response of SC2Hel in 50 mM TEA (pH 7.6), 150 mM NaCl at 22 °C. (a) The UV–visible absorption spectra are shown for the formation of INT-formazan ( $\lambda_{\max} = 505$  nm) during a SC2Hel reaction kinetics experiment at various time points: (i) 872 s, (ii) 752 s, (iii) 632 s, (iv) 512 s, (v) 392 s, (vi) 272 s, (vii) 152 s, and (viii) 32 s. The substrate concentrations were as follows: [dsDNA] = 17.9  $\mu$ M and [ATP] = 1.78 mM. (b) A plot of [INT-formazan] vs. time (red trace) is presented for the same kinetics experiment as in (a). The tangent line that was made from the first five time points ( $R^2 = 0.9995$ ) revealed a departure from the time trace plot and represented the linear regime of the reaction. The time optimum was determined to be 600 s. Michaelis–Menten plots of the SC2Hel/INT assay are shown for the formation rates of INT-formazan as a function of (c) [dsDNA] and (d) [ATP]. The mean and SD of three independent experiments are shown in both plots. The  $K_M$  value for the 31/18-mer dsDNA substrate was determined to be  $10.7 \pm 4.7$   $\mu$ M with a  $V_{\max}$  value of  $8.571 \times 10^{-3} \pm 1.938 \times 10^{-3}$  mM min<sup>-1</sup>  $\mu$ g prot<sup>-1</sup>. The  $K_M$  value for ATP was determined to be  $0.367 \pm 0.120$  mM with a  $V_{\max}$  value of  $1.932 \times 10^{-2} \pm 2.872 \times 10^{-3}$  mM min<sup>-1</sup>  $\mu$ g prot<sup>-1</sup>. In panel (c), the assay used various concentrations of the 31/18-mer dsDNA substrate (range of 0.625–20.0  $\mu$ M) and a constant concentration of ATP (2.00 mM). In panel (d), the assay used various concentrations of ATP (range of 0.0156–1.00 mM) and a constant concentration of 31/18-mer dsDNA substrate (72.0  $\mu$ M). In all cases, the final assay concentration of SC2Hel was  $1.3 \times 10^{-8}$  mol/L, experiments were performed at 22 °C, and the reaction time was 10.0 min. Data analysis and plots were prepared in *GraphPad Prism*.

### 3.2. Enzyme Activity of SC2Hel

We report on the Michaelis–Menten parameters for SC2Hel using a 31/18-mer dsDNA substrate with a  $K_M$  of  $10.7 \pm 4.7 \mu\text{M}$ , a  $V_{\text{MAX}}$  of  $8.571 \times 10^{-3} \pm 1.938 \times 10^{-3} \text{ mM min}^{-1} \mu\text{g prot}^{-1}$ , a  $k_{\text{cat}}$  of  $560 \pm 190 \text{ min}^{-1}$ , and a  $k_{\text{cat}}/K_M$  of  $69 \pm 15 \mu\text{M}^{-1} \text{ min}^{-1}$  (Figure 4c). For ATP, we report a  $K_M$  of  $0.367 \pm 0.120 \text{ mM}$ , a  $V_{\text{MAX}}$  of  $1.932 \times 10^{-2} \pm 2.872 \times 10^{-3} \text{ mM min}^{-1} \mu\text{g prot}^{-1}$ , a  $k_{\text{cat}}$  of  $1400 \pm 460 \text{ min}^{-1}$ , and a  $k_{\text{cat}}/K_M$  of  $4800 \pm 2800 \text{ mM}^{-1} \text{ min}^{-1}$  (Figure 4d). The SC2Hel  $K_M$  (31/18-mer dsDNA) in this study was found to be 4.1-fold higher than a previously reported SC2Hel  $K_M$  of  $2.6 \mu\text{M}$ , in which a slightly different nucleic acid substrate (35/15-mer dsDNA) was used; moreover, our determined SC2Hel  $K_M$  value with respect to ATP was 3.3-fold higher than their reported value of  $0.11 \text{ mM}$  [8]. The SC2Hel assay was performed at a pH of 7.6 and this pH value was important to maintain, particularly in the case of creating the standard curve. INT-formazan can be dissolved in DMSO, but it must be mixed with a buffered solution at pH 7.6 in order to achieve the same pH as was used in the assay. The assay included control experiments where SC2Hel was not added into the reaction mixture. In this case, there was residual production of INT-formazan, which can be attributed to the spontaneous degradation of ATP over time into ADP +  $P_i$ . The formed ADP appears to have proceeded into the reaction (2) of Figure 1. In data processing, the mean absorbance signal observed from three of these controls was assessed and background subtracted to obtain the amount of INT-formazan produced from the helicase assay. In general, the residual production of INT-formazan was not that extensive in our study because very pure ATP was used. Aliquots of a prepared ATP solution (dissolved in deionized ultrapure water) were frozen at  $-80 \text{ }^\circ\text{C}$  and our working solutions were used immediately on the day of the experiment after being thawed out on ice.

### 3.3. SC2Hel Assay Validation Parameters and the Suitability for HTS Experimentation

To interrogate the assay's validation parameters, seven replicates of positive and negative controls were inspected. All samples were run at an incubation time of 600 s at room temperature. We observed a signal-to-noise ratio and signal-to-background ratio of 439 and 294, respectively, which are very high and acceptable values. Additional assay parameters were calculated as described by Zhang and colleagues [19] and by Iversen and colleagues [20]. These parameters included a signal window of 21.5, an assay variability ratio of 0.13, and a  $Z'$  factor of 0.87. From the observation of positive and negative controls having exhibited very low variability, a high signal-to-noise, and a high  $Z'$  factor, we concluded that this assay demonstrated excellent performance characteristics. In particular, when  $Z'$  factor values are close to the value of 1.0 and much greater than 0.5, it is an important indicator for validating screening assays [19]. This criterion, on one hand, is based on signal quality in the absence of screening compounds (i.e., inhibitors); however, on the other hand, it is based on how well the coupled enzymes of ADP detection handle interference, such as chemical Equations (2)–(4) (as shown in Figure 1). HTS assays have routinely been performed by using some [21–24] or even all three [25] of these coupling steps, where interference was not considered to be unfavorable.

## 4. Conclusions

By using helicase nsp13 from SARS-CoV-2, we have demonstrated a simplistic colorimetric enzymatic assay that detects the presence of ADP resulting from nucleic acid unwinding (using a 31/18-mer dsDNA substrate) and ATPase activities. This assay is advantageous because it appears to be easier to employ compared to the traditional FRET-based helicase assay and it is rapid, sensitive, and colorimetric. Finally, the calculated high  $Z'$  factor of 0.87 strongly suggests that this assay has the potential to be configured for use in therapeutic drug discovery HTS screening studies.

**Author Contributions:** Conceptualization, E.L.D.; data curation T.M.P., M.G.H., S.M.C., L.R.B., and E.L.D.; formal analysis, T.M.P., M.G.H., S.M.C., L.R.B., and E.L.D.; funding acquisition, E.L.D.; investigation, E.L.D.; methodology, T.M.P., M.G.H., S.M.C., L.R.B., and E.L.D.; project administration, E.L.D.; resources, E.L.D.; software, E.L.D.; supervision, E.L.D.; validation, E.L.D.; visualization, E.L.D.; writing—original draft, T.M.P., M.G.H., S.M.C., L.R.B., and E.L.D.; writing—review & editing, T.M.P., M.G.H., S.M.C., L.R.B., and E.L.D.. All authors have read and agreed to the published version of the manuscript.

**Funding:** This research was funded by the University of South Carolina, Office of the Vice President for Research (proposal no. 925600-21-56127), Experiment.com (<https://doi.org/10.18258/17321> (accessed on 14 March 2024)), and the Shirley E. Caputo Memorial Fund from the Community Foundation of the Lowcountry (Hilton Head Island, SC) to Edward L. D’Antonio.

**Data Availability Statement:** Data pertaining to key findings is contained within the article.

**Acknowledgments:** We thank Gustavo F. Mercaldi at Laboratório Nacional de Biociências (LNBio) of Centro Nacional de Pesquisa em Energia e Materiais (CNPEM) in Campinas, São Paulo, Brazil for technical support.

**Conflicts of Interest:** The authors declare no conflict of interest.

## Abbreviations

COVID-19, Coronavirus Disease 2019; CkDIA, *Clostridium kluyveri* diaphorase; DMSO, dimethyl sulfoxide; DNase I, deoxyribonuclease I; F.A.C., final assay concentration; FRET, fluorescence resonance energy transfer; G6PDH, glucose-6-phosphate dehydrogenase; HEPES, 4-(2-hydroxyethyl)piperazine-1-ethanesulfonic acid; HTS, high-throughput screening; INT, iodonitrotetrazolium chloride; INT-formazan, iodonitrotetrazolium formazan; LmG6PDH, *Leuconostoc mesenteroides* glucose-6-phosphate dehydrogenase; LB, Luria–Bertani; MP, mobile phase; nsp, non-structural protein; RNase A, ribonuclease A; SARS-CoV-2, Severe Acute Respiratory Syndrome Coronavirus 2; SC2Hel, SARS-CoV-2 helicase; TIGlcK, *Thermococcus litoralis* glucokinase.

## References

1. World Health Organization. Coronavirus Disease Homepage. Updated 10 May 2022. Available online: <https://www.who.int/emergencies/diseases/novel-coronavirus-2019/> (accessed on 1 December 2022).
2. Centers for Disease Control and Prevention. COVID-19 Homepage. Updated 29 December 2022. Available online: <https://www.cdc.gov/coronavirus/2019-ncov/> (accessed on 1 December 2022).
3. Mercaldi, G.F.; Bezerra, E.H.S.; Batista, F.A.H.; Tonoli, C.C.C.; Soprano, A.S.; Shimizu, J.F.; Nagai, A.; da Silva, J.C.; Filho, H.V.R.; do Nascimento Faria, J.; et al. Discovery and structural characterization of chicoric acid as a SARS-CoV-2 nucleocapsid protein ligand and RNA binding disruptor. *Sci. Rep.* **2022**, *12*, 18500. [[CrossRef](#)] [[PubMed](#)]
4. Owen, D.R.; Allerton, C.M.N.; Anderson, A.S.; Aschenbrenner, L.; Avery, M.; Berritt, S.; Boras, B.; Cardin, R.D.; Carlo, A.; Coffman, K.J.; et al. An oral SARS-CoV-2 M<sup>PRO</sup> inhibitor clinical candidate for the treatment of COVID-19. *Science* **2021**, *374*, 1586–1593. [[CrossRef](#)] [[PubMed](#)]
5. Beigel, J.H.; Tomashek, K.M.; Dodd, L.E.; Mehta, A.K.; Zingman, B.S.; Kalil, A.C.; Hohmann, E.; Chu, H.Y.; Luetkemeyer, A.; Kline, S.; et al. Remdesivir for the treatment of COVID-19—Final report. *N. Engl. J. Med.* **2020**, *383*, 1813–1826. [[CrossRef](#)]
6. Jayk Bernal, A.; Gomes da Silva, M.M.; Musungaie, D.B.; Kovalchuk, E.; Gonzalez, A.; Delos Reyes, V.; Martín-Quirós, A.; Caraco, Y.; Williams-Diaz, A.; Brown, M.L.; et al. Molnupiravir for oral treatment of Covid-19 in nonhospitalized patients. *N. Engl. J. Med.* **2021**, *386*, 509–520. [[CrossRef](#)]
7. Yoshimoto, F.K. The proteins of Severe Acute Respiratory Syndrome Coronavirus-2 (SARS CoV-2 or n-COV19), the cause of COVID-19. *Protein J.* **2020**, *39*, 198–216. [[CrossRef](#)] [[PubMed](#)]
8. Zeng, J.; Weissmann, F.; Bertolin, A.P.; Posse, V.; Canal, B.; Ulferts, R.; Wu, M.; Harvey, R.; Hussain, S.; Milligan, J.C.; et al. Identifying SARS-CoV-2 antiviral compounds by screening for small molecule inhibitors of nsp13 helicase. *Biochem. J.* **2021**, *478*, 2405–2423. [[CrossRef](#)]
9. White, M.A.; Lin, W.; Cheng, X. Discovery of COVID-19 inhibitors targeting the SARS-CoV-2 nsp13 helicase. *J. Phys. Chem. Lett.* **2020**, *11*, 9144–9151. [[CrossRef](#)]
10. Newman, J.A.; Douangamath, A.; Yadzani, S.; Yosaatmadja, Y.; Aimon, A.; Brandão-Neto, J.; Dunnett, L.; Gorrie-Stone, T.; Skyner, R.; Fearon, D.; et al. Structure, mechanism and crystallographic fragment screening of the SARS-CoV-2 NSP13 helicase. *Nat. Commun.* **2021**, *12*, 4848. [[CrossRef](#)]
11. Adedeji, A.O.; Marchand, B.; te Velthuis, A.J.W.; Snijder, E.J.; Weiss, S.; Eoff, R.L.; Singh, K.; Sarafianos, S.G. Mechanism of nucleic acid unwinding by SARS-CoV helicase. *PLoS ONE* **2012**, *7*, e36521. [[CrossRef](#)]

12. Adedeji, A.O.; Singh, K.; Calcaterra, N.E.; DeDiego, M.L.; Enjuanes, L.; Weiss, S.; Sarafianos, S.G. Severe acute respiratory syndrome coronavirus replication inhibitor that interferes with the nucleic acid unwinding of the viral helicase. *Antimicrob. Agents Chemother.* **2012**, *56*, 4718–4728. [[CrossRef](#)]
13. Tanner, J.A.; Watt, R.M.; Chai, Y.; Lu, L.; Lin, M.C.; Peiris, J.S.M.; Poon, L.L.M.; Kung, H.; Huang, J. The severe acute respiratory syndrome (SARS) coronavirus NTPase/helicase belongs to a distinct class of 5' to 3' viral helicases. *J. Biol. Chem.* **2003**, *278*, 39578–39582. [[CrossRef](#)]
14. Jia, Z.; Yan, L.; Ren, Z.; Wu, L.; Wang, J.; Guo, J.; Zheng, L.; Ming, Z.; Zhang, L.; Lou, Z.; et al. Delicate structural coordination of the Severe Acute Respiratory Syndrome coronavirus nsp13 upon ATP hydrolysis. *Nucleic Acids Res.* **2019**, *47*, 6538–6550. [[CrossRef](#)] [[PubMed](#)]
15. Lohman, T.M.; Tomko, E.J.; Wu, C.G. Non-hexameric DNA helicases and translocases: Mechanisms and regulation. *Nat. Rev. Mol. Cell Biol.* **2008**, *9*, 391–401. [[CrossRef](#)]
16. Mickolajczyk, K.J.; Shelton, P.M.M.; Grasso, M.; Cao, X.; Warrington, S.E.; Aher, A.; Liu, S.; Kapoor, T.M. Force-dependent stimulation of RNA unwinding by SARS-CoV-2 nsp13 helicase. *Biophys. J.* **2021**, *120*, 1020–1030. [[CrossRef](#)] [[PubMed](#)]
17. McFarlane, C.R.; Murray, J.W. A sensitive coupled enzyme assay for measuring kinase and ATPase kinetics using ADP-specific hexokinase. *Bio-Protocol* **2020**, *10*, e3599. [[CrossRef](#)] [[PubMed](#)]
18. Gill, S.C.; von Hippel, P.H. Calculation of protein extinction coefficients from amino acid sequence data. *Anal. Biochem.* **1989**, *182*, 319–326. [[CrossRef](#)] [[PubMed](#)]
19. Zhang, J.H.; Chung, T.D.Y.; Oldenburg, K.R. A simple statistical parameter for use in evaluation and validation of high throughput screening assays. *J. Biomol. Screen.* **1999**, *4*, 67–73. [[CrossRef](#)] [[PubMed](#)]
20. Iversen, P.W.; Eastwood, B.J.; Sittampalam, G.S.; Cox, K.L. A comparison of assay performance measures in screening assays: Signal window, Z' factor, and assay variability ratio. *J. Biomol. Screen.* **2006**, *11*, 247–252. [[CrossRef](#)]
21. Mercaldi, G.F.; D'Antonio, E.L.; Aguessi, A.; Rodriguez, A.; Cordeiro, A.T. Discovery of antichagasic inhibitors by high-throughput screening with *Trypanosoma cruzi* glucokinase. *Bioorg. Med. Chem. Lett.* **2019**, *29*, 1948–1953. [[CrossRef](#)]
22. Mercaldi, G.F.; Ranzani, A.T.; Cordeiro, A.T. Discovery of new uncompetitive inhibitors of glucose-6-phosphate dehydrogenase. *J. Biomol. Screen.* **2014**, *19*, 1362–1371. [[CrossRef](#)]
23. Mota, S.G.R.; Mercaldi, G.F.; Pereira, J.G.C.; Oliveira, P.S.L.; Rodriguez, A.; Cordeiro, A.T. First nonphosphorylated inhibitors of phosphoglucose isomerase identified by chemical library screening. *SLAS Discov.* **2018**, *23*, 1051–1059. [[CrossRef](#)] [[PubMed](#)]
24. Ranzani, A.T.; Nowicki, C.; Wilkinson, S.R.; Cordeiro, A.T. Identification of specific inhibitors of *Trypanosoma cruzi* malic enzyme isoforms by target-based HTS. *SLAS Discov.* **2017**, *22*, 1150–1161. [[CrossRef](#)] [[PubMed](#)]
25. Imamura, R.M.; Kumagai, K.; Nakano, H.; Okabe, T.; Nagano, T.; Kojima, H. Inexpensive high-throughput screening of kinase inhibitors using one-step enzyme-coupled fluorescence assay for ADP detection. *SLAS Discov.* **2019**, *24*, 284–294. [[CrossRef](#)] [[PubMed](#)]

**Disclaimer/Publisher's Note:** The statements, opinions and data contained in all publications are solely those of the individual author(s) and contributor(s) and not of MDPI and/or the editor(s). MDPI and/or the editor(s) disclaim responsibility for any injury to people or property resulting from any ideas, methods, instructions or products referred to in the content.